How Ecology and Landscape Dynamics Shape Phylogenetic Trees

FANNY GASCUEL[1,2,3,*], RÉGIS FERRIÈRE[3,4,+], ROBIN AGUILÉE[5], AND AMAURY LAMBERT[1,6,+]

[1] Center for Interdisciplinary Research in Biology, CNRS UMR 7241, Collège de France, Paris, France ;

[2] Sorbonne Universités, UPMC Univ Paris 06, CNRS UMR 7625, Laboratoire Écologie et Évolution, Paris, France ;

[3] Institut de Biologie de l'Ecole Normale Supérieure, CNRS UMR 8197, École Normale Supérieure, Paris, France ;

[4] Department of Ecology and Evolutionary Biology, University of Arizona, Tucson, USA ;

[5] Laboratoire Évolution et Diversité Biologique, CNRS UMR 5174, Université Paul Sabatier, Toulouse, France ;

[6] Sorbonne Universités, UPMC Univ Paris 06, CNRS UMR 7599, Laboratoire Probabilités et Modèles Aléatoires, Paris, France

[*] **Corresponding author :** Fanny Gascuel, Center for Interdisciplinary Research in Biology, Equipe Stochastic Models for the Inference of Life Evolution, Collège de France, 11 place Marcelin Berthelot, 75005 Paris, France ; E-mail : fanny.gascuel@college-de-france.fr.

APPENDIX

Appendix 1 : Sensitivity of phylogenetic tree shape to migration rate across connected sites

In our main model, migration is uniform among connected geographical sites, i.e. connected sites are panmictic and species therein evolve in sympatry. We tested for the importance of this assumption by considering another version of the model where, within sets of connected sites, migration is more likely towards the sites where the offspring's parents are located than towards other sites (parapatry). Figure A1 shows that this assumption has no major influence on the shape of phylogenetic trees.
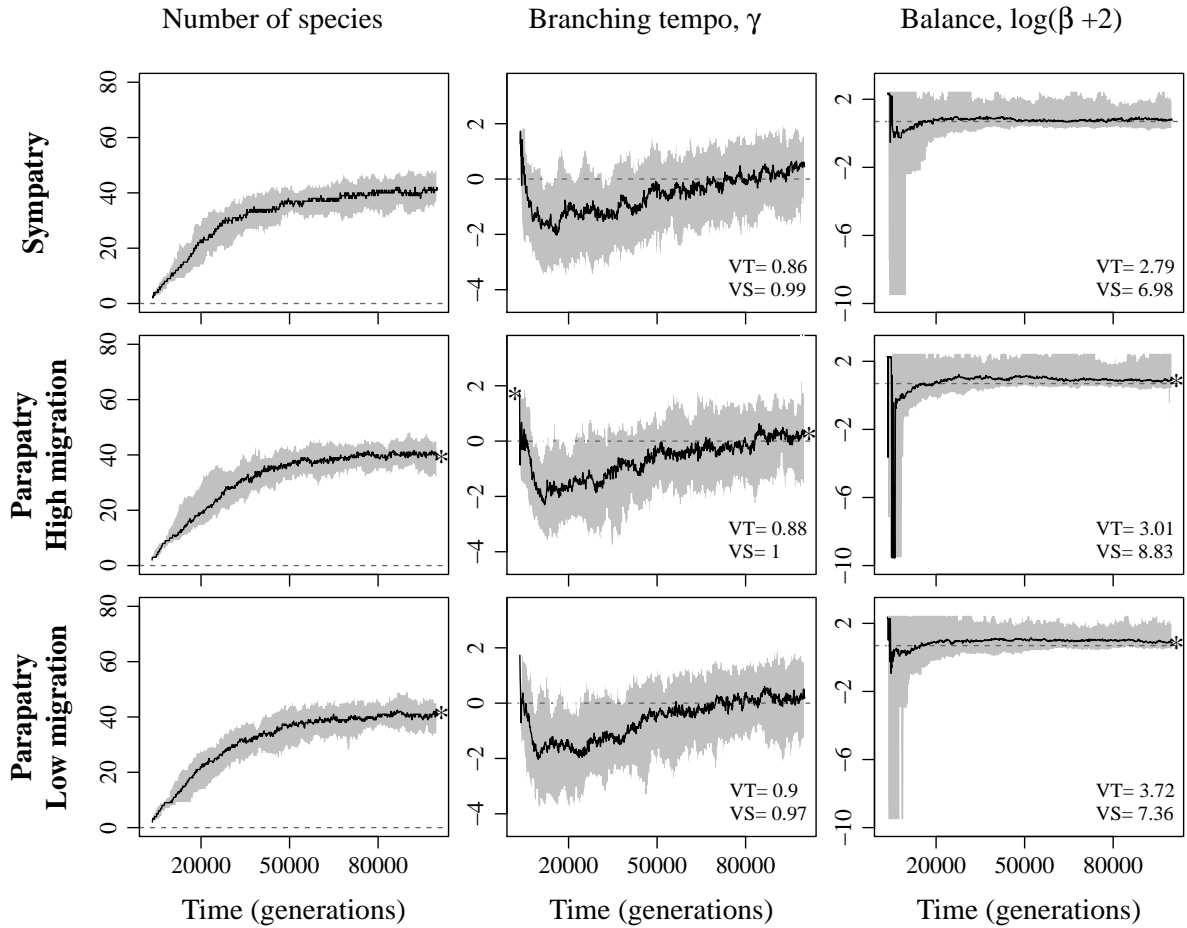
FIGURE A1 – Effect of the probability of migration at birth among connected sites on the evolution of species diversity, branching tempo γ and balance β of phylogenetic trees through time. Time is measured from the introduction of the ancestral species in the landscape. Probability of migration at birth, p, decreases from top to bottom : p=1.0 (sympatry), p=0.8 (parapatry with high migration probability), and p=0.6 (parapatry with low migration probability). Data was computed over 50 simulation replicates. Black lines show the median values and grey areas give the 95% confidence interval. Dashed horizontal lines show γ=0 and β=0. VT and VS give the average variance, respectively over time (corrected according to the median among simulation replicates) and among simulation replicates. Stars show the statistical differences ($p-value$ <0.05, t-test) with results with sympatry, either at the beginning or at the end (respectively first and last 20,000 generations) of the simulations. See Table 1 for other parameter values.

Appendix 2 : Sensitivity of phylogenetic tree shape to the approximation on the reproductive isolation between populations

　　We verified that computing the probability of reproductive isolation between pairs of populations using their average trait values $\overline{x_1}$, $\overline{x_2}$ and $\overline{a}$, which reduces computation time significantly, does not affect our results. Indeed, exact probabilities of reproductive isolation between populations should be calculated as the average of the probability of reproductive isolation between each pair of individuals from both populations. We therefore compared the temporal patterns of variation in phylogenetic tree shape obtained using the approximation to those expected without approximation : Figure A2 shows that considering the mean trait values of populations does not strongly modify the shape of reconstructed species trees.
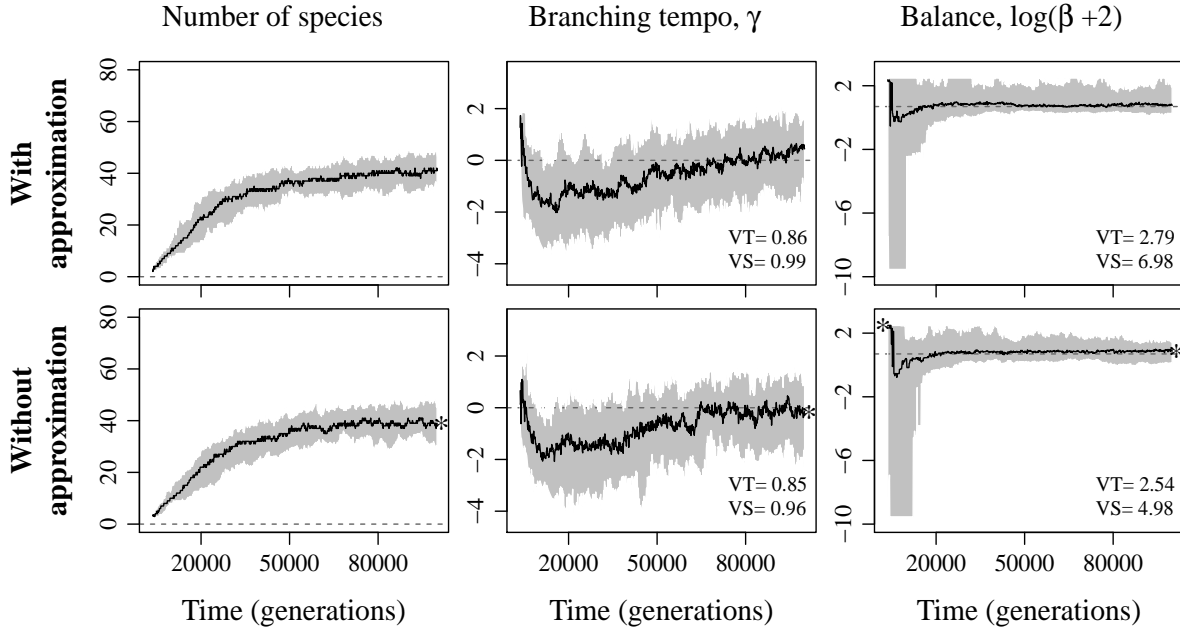
FIGURE A2 – Effect of approximating the probability of reproductive isolation between pairs of populations on the evolution of species diversity, branching tempo γ and balance β of phylogenetic trees through time. Time is measured from the introduction of the ancestral species in the landscape. In the top row, probabilities of reproductive isolation between pairs of populations were approximated using the mean trait values of populations, whereas in the bottom row they were calculated exactly as the mean over the probabilities of reproductive isolation between each pair of individuals of both populations. Data was computed over 50 simulation replicates. Black lines show the median values and grey areas give the 95% confidence intervals. Dashed horizontal lines show γ=0 and β=0. VT and VS give the average variance, respectively over time (corrected according to the median among simulation replicates) and among simulation replicates. Stars show the statistical differences ($p-value$ <0.05, t-test) between both sets of results, either at the beginning or at the end (respectively first and last 20,000 generations) of the simulations. See Table 1 for other parameter values.

We verified that the frequency at which we compute the existing species and identify their origin during the course of diversification was high enough to enable a precise determination of the relationships between species. Figure A3 shows that the time step of 100 generations that we chose leads to quite similar results as a time step of 10 generations : it is short enough to accurately capture real phylogenetic tree shapes.
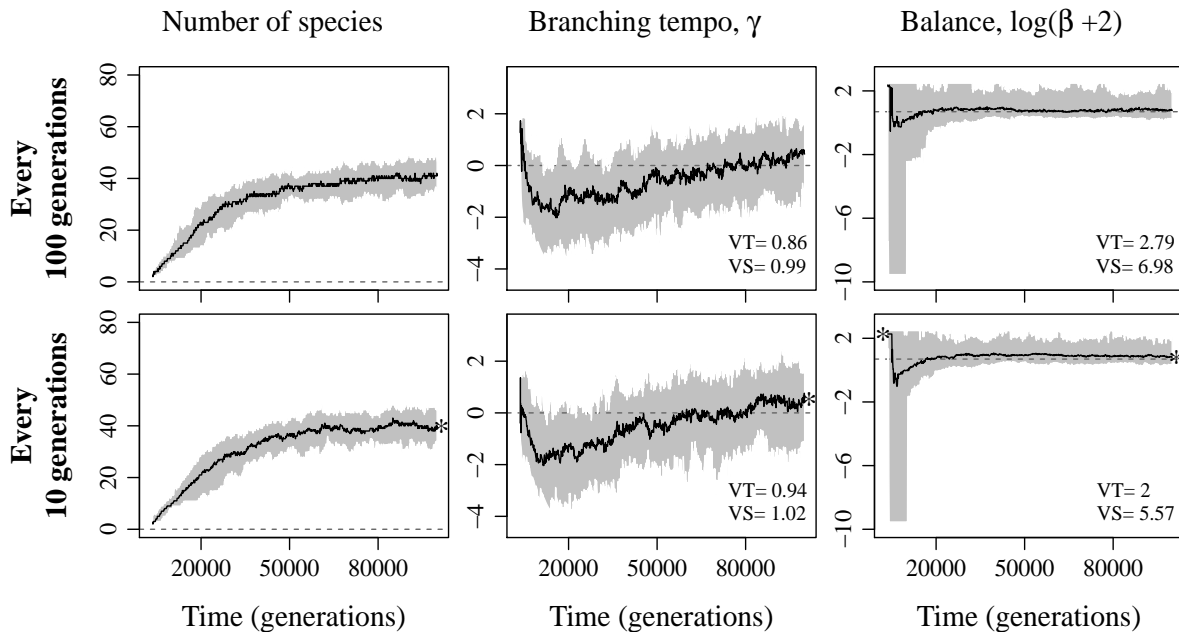
FIGURE A3 – Effect of the time interval between each species identification on the evolution of species diversity, branching tempo γ and balance β of phylogenetic trees through time. Time is measured from the introduction of the ancestral species in the landscape. In the top row, species were identified every 100 generations (default value), and in the bottom row, every 10 generations. Data was computed over 50 simulation replicates. Black lines show the median values and grey areas give the 95% confidence intervals. Dashed horizontal lines show $\gamma=0$ and $\beta=0$. VT and VS give the average variance, respectively over time (corrected according to the median among simulation replicates) and among simulation replicates. Stars show the statistical differences ($p-value$ <0.05, t-test) between both sets of results, either at the beginning or at the end (respectively first and last 20,000 generations) of the simulations. See Table 1 for other parameter values.

Appendix 4 : Delineating species and following their evolutionary history

To follow the evolutionary history of species and determine the phylogenetic tree generated during diversification, at each time step t (typically every 100 generations), we first delineate the N_t existing species $[S_t^{(i)}]_{i \in \{1,...,N_t\}}$ (Fig. A4), and then determine their ancestry relatively to the species $[S_{t-1}^{(j)}]_{j \in \{1,...,N_{t-1}\}}$ existing at the previous time step (Fig. A5).
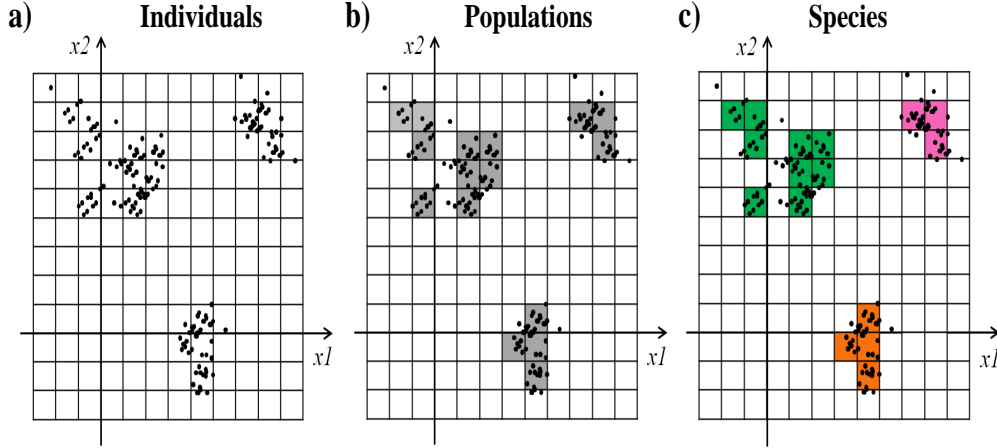
FIGURE A4 – To delineate species, we (a) extract the distribution of all individuals in the phenotypic space (x_1, x_2), according to cells of width $\sigma_{\mu_{x_1}} \times \sigma_{\mu_{x_2}}$; (b) determine high density phenotypic cells, and group individuals within adjacent high density cells into populations; (c) group populations that can interbreed (probability of reproductive isolation below the threshold thr_{ri}=99%) into species, using their average ecological and choosiness traits ($\overline{x_1}$, $\overline{x_2}$, $\overline{a}$; calculated over all their individuals) and the same function as for mating between individuals.

In this second step (Fig. A5), our algorithm proceeds as follows. Because each species $S_t^{(i)}$ is a set of populations, we start by determining the identity of all these populations. This identity is the one of the most ecologically similar population at time $t-1$ (based on mean ecological traits $\overline{x_1}$ and $\overline{x_2}$). If all the populations included into species $S_t^{(i)}$ have the same species identity $S_{t-1}^{(j)}$, $S_t^{(i)}$ takes this identity. However, if species $S_t^{(i)}$ includes populations with different species identities $[S_{t-1}^{(j)}]_{j \in \{1,...,N_{t-1}\}}$, hybridization has occurred, and we fix the identity of $S_t^{(i)}$ as the one of the ecologically most similar of these previous species $[S_{t-1}^{(j)}]_{j \in \{1,...,N_{t-1}\}}$. Those containing more individuals are more likely to be closer to $S_t^{(i)}$ and thus to transmit their identity (consistently with their higher probability to transmit their genotype to the lineage descending from $S_t^{(i)}$). Once identities have been attributed to each species $[S_t^{(i)}]_{i \in \{1,...,N_t\}}$, we check that two or more different
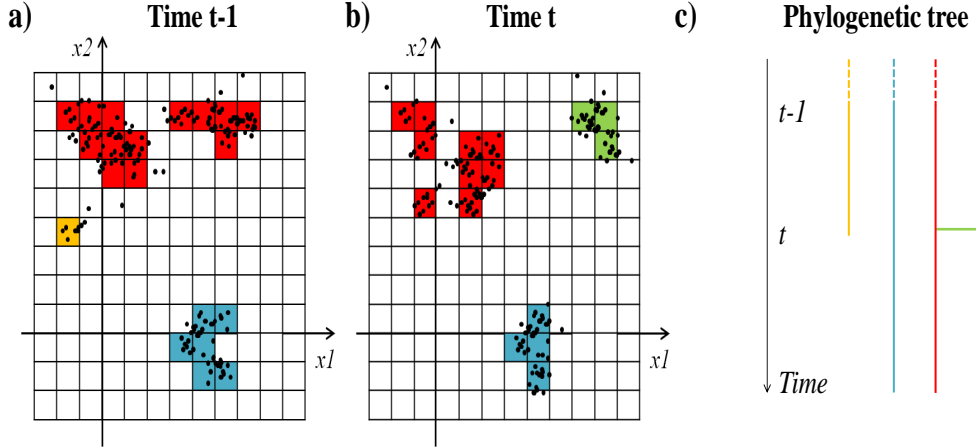
FIGURE A5 – To determine the ancestry of the species $[S_t^{(i)}]_{i \in \{1,...,N_t\}}$ delineated at time step t (as presented in Fig. A4), and thus the changes in the phylogenetic tree between time step $t-1$ and time step t (c), we compare the phenotypic traits of species and populations at time t (b) to those at time $t-1$ (a). Descent relationships are determined by minimum Euclidian distances between average traits of entities at time t and at time $t-1$. Speciation occurs if different species $S_t^{(i)}$ descend from the same species $S_{t-1}^{(j)}$; in that case (e.g. the red and green species at time t), the species $S_t^{(i)}$ most similar to $S_{t-1}^{(j)}$ is $S_{t-1}^{(j)}$ (here the red species), whereas other species $S_t^{(i)}$ (here the green species) are new ones, descending from $S_{t-1}^{(j)}$. Hybridization occurs if a species $S_t^{(i)}$ includes populations descending from populations of several different species $S_{t-1}^{(j)}$; in that case $S_t^{(i)}$ (e.g. the red species at time t), has evolved from the most similar of its parental species $S_{t-1}^{(j)}$ (here the red species), partly due to hybridization, whereas other species $S_{t-1}^{(j)}$ (here the yellow species) might go extinct.

species do not have the same identity. If several species $[S_t^{(i)}]_{i \in \{1,...,N_t\}}$ have the same identity $S_{t-1}^{(j)}$, speciation has occurred between time $t-1$ and time t. We therefore update their identity by calculating their phenotypic distance to $S_{t-1}^{(j)}$: only the most similar species keeps the identity of $S_{t-1}^{(j)}$, all other species being new ones descending from $S_{t-1}^{(j)}$.

Appendix 5 : Competition width and phylogenetic tree shape in the presence of border effects

       In the default conditions, the ecological and assortative mating traits (x_1, x_2 and a) of the ancestral species were determined by L_k, $k \in \{x_1, x_2, a\}$, diploid loci randomly chosen in a Gaussian distribution centered at zero. The ecological optima (x_1^*, x_2^*) of the 9 geographical sites were taken in $\{-1,0,1\} \times \{-1,0,1\}$. Thus, the ancestral species was rather well adapted to the central geographical site.

       We explored the influence of border effects acting during early diversification, by considering an ancestral species adapted to marginal ecological conditions. In that case, the ecological and assortative mating traits (x_1, x_2 and a) of the ancestral species were determined by L_k, $k \in \{x_1, x_2, a\}$, diploid loci randomly chosen in a Gaussian distribution centered at one. The ancestral species was thus rather well adapted to the geographical site with ecological optimum ($x_1^*=1$, $x_2^*=1$).

       Results show that border effects influence the shape of phylogenetic trees, both initially and at steady state. First, γ exhibit less temporal variation, because the initial allopatric radiation is more gradual : all allopatric speciations do not occur so closely in time. The initial allopatric radiation is therefore not so decoupled from diversification due to landscape dynamics. Second, β is more variable but on average less negative initially, and therefore does not stay negative at steady state in clades undergoing wide competition. Indeed, during the initial allopatric radiation, species originating in geographical sites located on the opposite side (e.g., with ecological optimum $x_1^*=-1$, $x_2^*=-1$) of the ancestral species do not descend from the latter, but from recent species with intermediate phenotypes, thus generating more balanced trees.
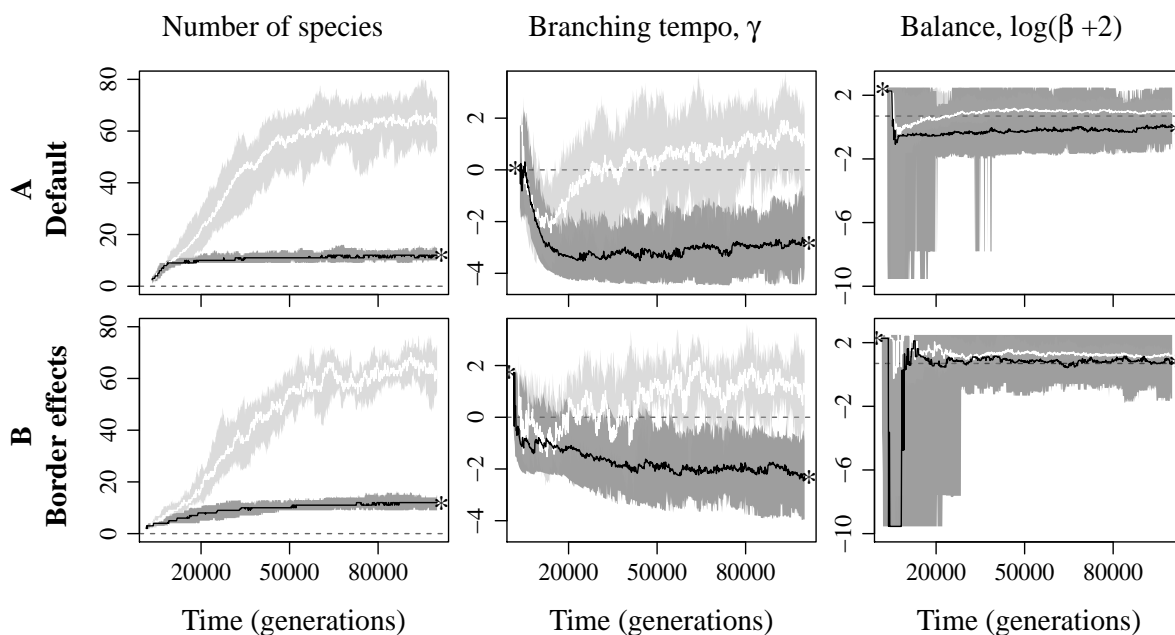
FIGURE A6 – How border effects alter the effect of the scaled width of competition on the evolution of species diversity, branching tempo γ and balance β of phylogenetic trees through time. Time is measured from the introduction of the ancestral species in the landscape. In row B, unlike in row A (default, from Fig.2.A), the early diversification was constrained by border effects (the ancestral species being adapted to marginal ecological conditions). Data was computed over 50 simulation replicates. Black lines surrounded by dark grey areas give the median and 95% confidence intervals under wide competition (σ_C/σ_K=0.75), while white lines and light grey areas give them under narrow competition (σ_C/σ_K=0.25). Stars show the statistical differences ($p-value$ <0.05, t-test) between results under wide and narrow competition, either at the beginning or at the end (respectively first and last 20,000 generations) of the simulations. Dashed horizontal lines show γ=0 and β=0. See Table 1 for other parameter values.

Appendix 6 : Hybridization and influence of irreversible reproductive isolation on phylogenetic tree shape

There is empirical evidence for the existence of hybrid collapse and hybrid speciation (e.g., Ungerer et al. 1998; Taylor et al. 2006; Behm et al. 2010; Elowsky et al. 2013; Hasselman et al. 2014; Kleindorfer et al. 2014), but mostly among species pairs. After some time, species are likely to evolve irreversible Dobzhansky-Muller genetic incompatibilities, which result from negative epistatic interactions between alleles that arose in independent genetic backgrounds, and prevent them from hybridizing or giving birth to a viable and fertile descent. In our model, we did not incorporate such long-term isolation mechanism. We indeed considered "reproductive isolation" between species to be based only on the divergence of ecological phenotypes and evolution of assortative mating traits. Because traits evolve, reproductive isolation is thus reversible. Hybridization can happen between species even if the latter diverged a long time before.

To explore the influence of hybridization on tree shape and species turnover at steady state (relatively to that of competition and demographic stochasticity) and to investigate tree dynamics uninfluenced by hybrid collapses, we developed a version of the model which accounts for irreversible reproductive isolation between species. We ran simulations under different competition width, σ_C/σ_K, because competition width have a strong effect on the proportion of simulations resulting in a hybrid collapse (the latter decreases with competition width), thus potential on the rate of species hybridization.

We incorporated this isolation mechanism by preventing reproduction between individuals (and thus hybridization between species) with high number of loci harbouring incompatible alleles. New born individuals inherit alleles from their parents following a random independent segregation of parental loci, and may acquire new alleles following an infinite site model, with mutation probability μ. According to previous mathematical analyses (Orr 1995; Orr and Turelli 2001) and empirical results (e.g., Matute et al. 2010; Moyle and Nakazato 2010), the number of incompatible genetic loci between two individuals, J, increases rapidly ("snow-ball" effect) with their genetic distance d (i.e. the number of different mutations that they carry) :

$$J = q\binom{d}{2},$$

where q is the probability of incompatibility between two loci, and $\binom{d}{2}$ is the number of pairs of loci among the d different loci which separate both individuals.

Following Gavrilets (2003), we computed the probability of reproductive isolation due to genetic incompatibilities between pairs of individuals, $Q(C, J)$, as a normalized incomplete gamma function of the expected number of incompatible genetic loci, J, with parameter C quantifying the threshold in number of incompatible loci needed to generate reproductive isolation (Fig. A7) :

$$Q(C, J) = 1/\Gamma(C) \int_J^\infty t^{C-1} \exp(-t)dt.$$
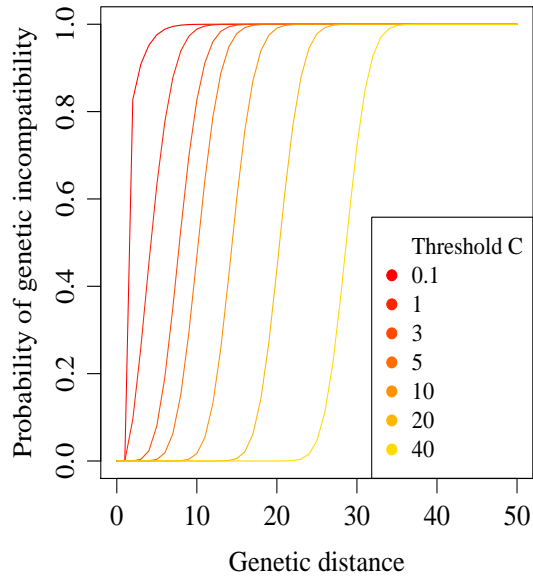
FIGURE A7 – Probability of genetic incompatibility $Q(C, J)$ as a (normalized incomplete Gamma function) of the genetic distance (number of different mutations) between pairs of individuals. Here, $q = 0.1$ $\mu = 8.10^{-5}$, d varies between 0 and 50, and C varies between 0.1 and 40.

We simulated diversification with the accumulation of genetic incompatibilities between lineages as explained above, using parameter values $\mu = 8.10^{-5}$, $q = 0.1$ and C varying between 0.1 and 40 (Fig. A7). These parameter values ensure that fully differentiated species cannot hybridize : the parameter C determines the genetic distance over which species are reproductively isolated and, for the smaller value we used ($C = 0.1$), only two mutations are likely to generate reproductive isolation (Fig. A7). These parameter values also ensure that reproductive isolation following from genetic incompatibilities does not contribute to speciation. Previous studies indeed showed that speciation rates are often decoupled from the rate of evolution of reproductive isolation (Rabosky and Matute 2013), and we are here interested in diversification driven by ecological speciation.

Results show that accounting for reproductive isolation due to the accumulation of genetic incompatibilities favors the persistence of diversity over long time scales, by preventing the generation of hybrid collapse (Fig. A8). However, accounting for genetic incompatibilities does not influence the effects of the scaled width of competition on phylogenetic tree shape (predicted in scenarios without hybrid collapse in the absence of genetic incompatibilities ; Fig. A9). Indeed, neither speciation nor extinction rates are influenced by the evolution of genetic incompatibilities (Fig. A10). On the one hand, even at low threshold C, genetic incompatibilities accumulate too slowly to increase speciation rate. On the other hand, if rather distant species hybridize, it always results in a hybrid collapse. Indeed, if distant species could hybridize without generating a hybrid collapse, one would expect that preventing hybridization between species that diverged not long ago (i.e. low threshold in the number of mutations needed to generate irreversible reproductive isolation C) would decrease the species turnover at steady state. As a result, we would expect an increase in speciation and extinction rate with the threshold C. On the contrary, we observe on Figure A10 that speciation and extinction rates are unaffected by the value

of C. This suggest that hybridization only occurs when diversification collapses into a hybrid swarm.

Two conclusions follow. First, considering only scenarios in which hybrid collapse does not occur (as we did) is akin to implementing long-term irreversible reproductive isolation between species. Second, in the absence of genetic incompatibilities, species turnover at equilibrium is not due to hybridization between species, but only to competition and demographic stochasticity.
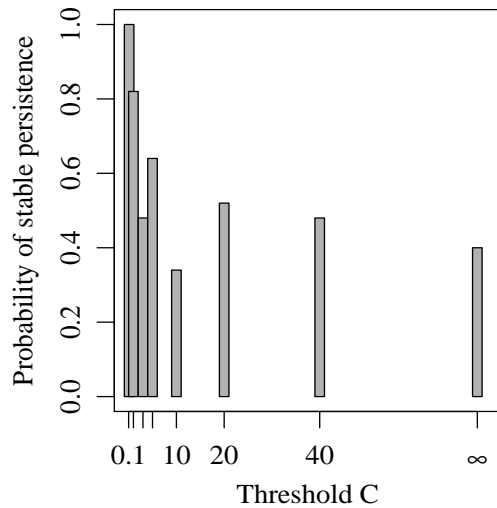
FIGURE A8 – Probability of stable persistence (no hybrid collapse in the 100,000 first generations) as a function of the threshold C of the number of incompatible loci needed to generate reproductive isolation. $C=\infty$ corresponds to simulations without genetic incompatibility. $\mu = 8.10^{-5}$, $q = 0.1$, $\sigma_C = 0.3$, and $\sigma_K = 1.2$. See Table 1 for other parameter values.
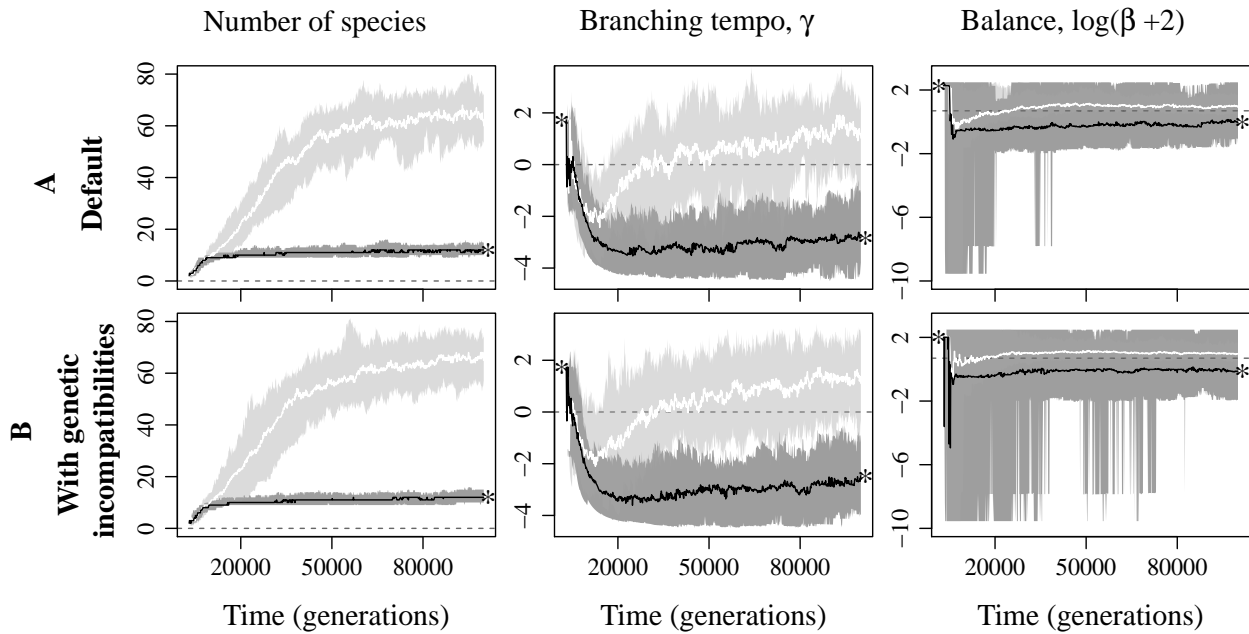
FIGURE A9 – Influence of long-term irreversible reproductive isolation due to genetic incompatibilities on the effect of the scaled width of competition on the evolution of species diversity, branching tempo γ and balance β of phylogenetic trees through time. Time is measured from the introduction of the ancestral species in the landscape. In row B, unlike in row A (default, from Fig.2.A), genetic incompatibilities generate long-term reproductive isolation between species. Data was computed over 50 simulation replicates. Black lines surrounded by dark grey areas give the median and 95% confidence intervals under wide competition (σ_C/σ_K=0.75), while white lines and light grey areas give them under narrow competition (σ_C/σ_K=0.25). Stars show the statistical differences ($p-value$ <0.05, t-test) between results under wide and narrow competition, either at the beginning or at the end (respectively first and last 20,000 generations) of the simulations. Dashed horizontal lines show γ=0 and β=0. These simulations were performed with $\mu = 8.10^{-5}$, $q = 0.1$, and $C = 0.1$. See Table 1 for other parameter values.
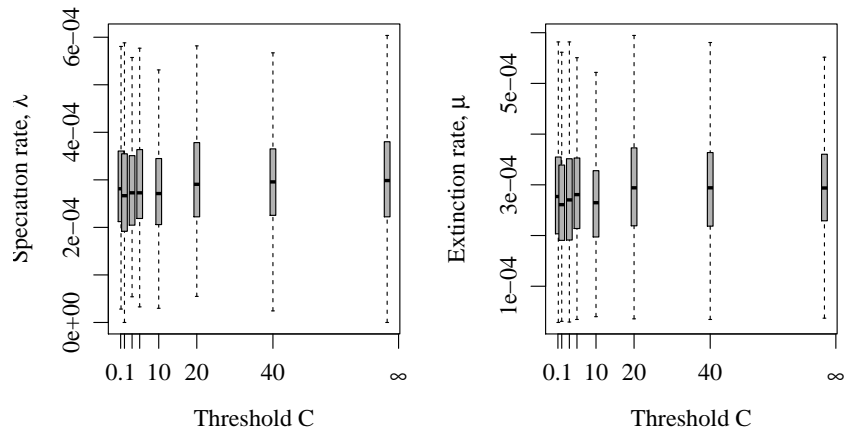
FIGURE A10 – (Per species) speciation (λ) and extinction (μ) rates at steady state as a function of the threshold C of the number of incompatible loci needed to generate reproductive isolation. Boxplots show the distribution of the median values during the last 10,000 generations of the simulations, calculated over 50 simulation replicates; vertical boxes represent the first, second and third quartiles, and whiskers give the upper and lower values (of maximum 1.5 times the interquartile distance). $C=\infty$ corresponds to simulations without genetic incompatibility. $\mu = 8.10^{-5}$, $q = 0.1$, $\sigma_C = 0.3$, and $\sigma_K = 1.2$ (parameter values associated with high probability of hybrid collapse). See Table 1 for other parameter values.

Appendix 7 : Variability in tree balance β and clade size

Figure A11 shows that the variability in the balance β of phylogenetic trees depends on clade size : under the birth-death process (Yule 1925; Kendall 1948; Raup et al. 1973), phylogenetic trees which contain few species exhibit higher variability in β values (Fig. A11). Moreover, very small clades are expected to be characterized by a positive median β value.
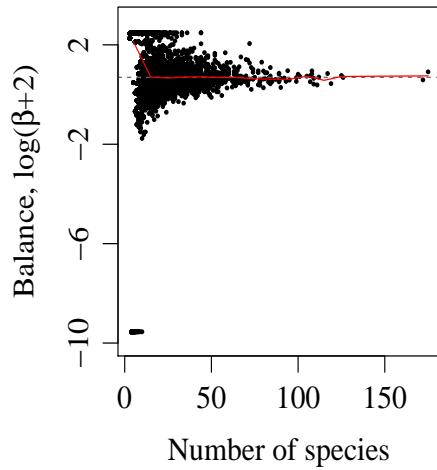
FIGURE A11 – Effect of clade size (number of species) on variability in the balance β of phylogenetic trees generated under the birth-death process. The dashed horizontal line shows $\beta=0$, and the red line shows the median value of β over time (computed on intervals of 10 units in species numbers). Trees were simulated on 50,000 time units, with birth rate = 0.0002 and death rate = 0.00018, using the R package (Harmon et al. 2008).

Appendix 8 : Non-linear relationship between competition width and phylogenetic tree shape at steady state

Branching tempo γ and the balance β of phylogenetic trees vary non linearly with the scaled width of competition : γ and β strongly decrease under the largest competition width (Fig. A12). Therefore, under spatial heterogeneity in competition width, γ and β may be driven downward by geographical sites in which competition is wider (i.e. having high σ_C/σ_K).
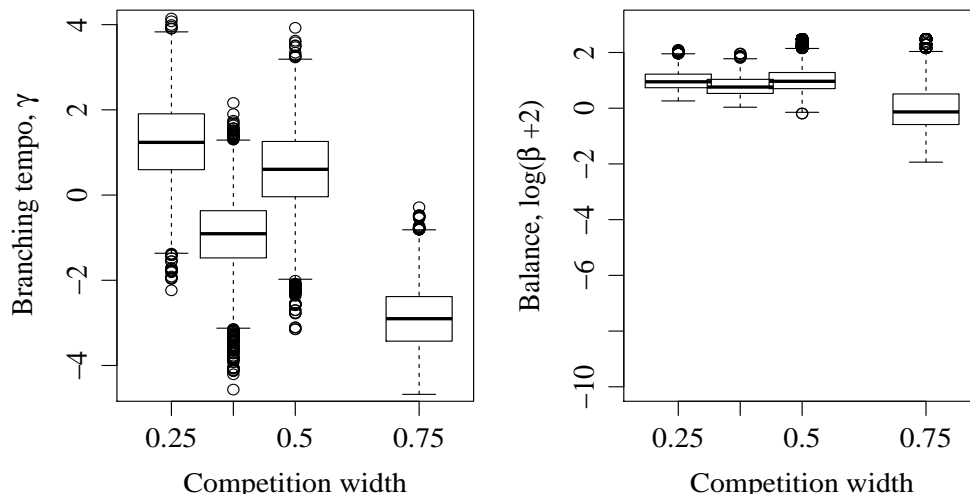
FIGURE A12 – Branching tempo γ and balance β of phylogenetic trees at steady state as a function of the scaled width of competition (i.e. σ_C/σ_K). Boxplots show the distribution of the median γ and β values during the last 20,000 generations of the simulations, calculated over 50 simulation replicates; vertical boxes represent the first, second and third quartiles, and whiskers give the upper and lower values (of maximum 1.5 times the interquartile distance). Data were obtained from simulations without spatial heterogeneity, with values of σ_C in {0.3, 0.6} and σ_K in {0.8, 1.2} (similar to those used with spatial heterogeneity in scaled competition width). See Table 1 for other parameter values.

Appendix 9 : Shape of real reconstructed species trees at the genus level

Here we search for patterns in the shape of real phylogenetic trees at the genus level, at which all species are assumed to share the same trophic level, and competition is potentially significant. We extracted recently published phylogenies of genera and characterized their shape in terms of branching tempo γ and balance β. We used phylogenies published by Phillimore and Price (2008), McPeek (2008), Jetz et al. (2012) and Bininda-Emonds et al. (2007), accounting for different groups of living organisms. We excluded all phylogenies of genera which contained less than 5 species or had less than two thirds of their nodes resolved. This led us to use 621 phylogenetic trees.

We found that, as for trees not limited to genera (Nee et al. 1992; Pybus and Harvey 2000; McPeek 2008; Guyer and Slowinski 1991, 1993; Mooers 1995; Blum and François 2006), most genus-level phylogenies have negative γ and negative β (Fig.A13). However, γ and β show large variation (Fig.A13). A substantial fraction of trees have negative γ and positive β (including many estimates of β at its upper limit, 10), consistent with a pattern of evolution under short isolation time, or recent diversification in the presence of border effects.
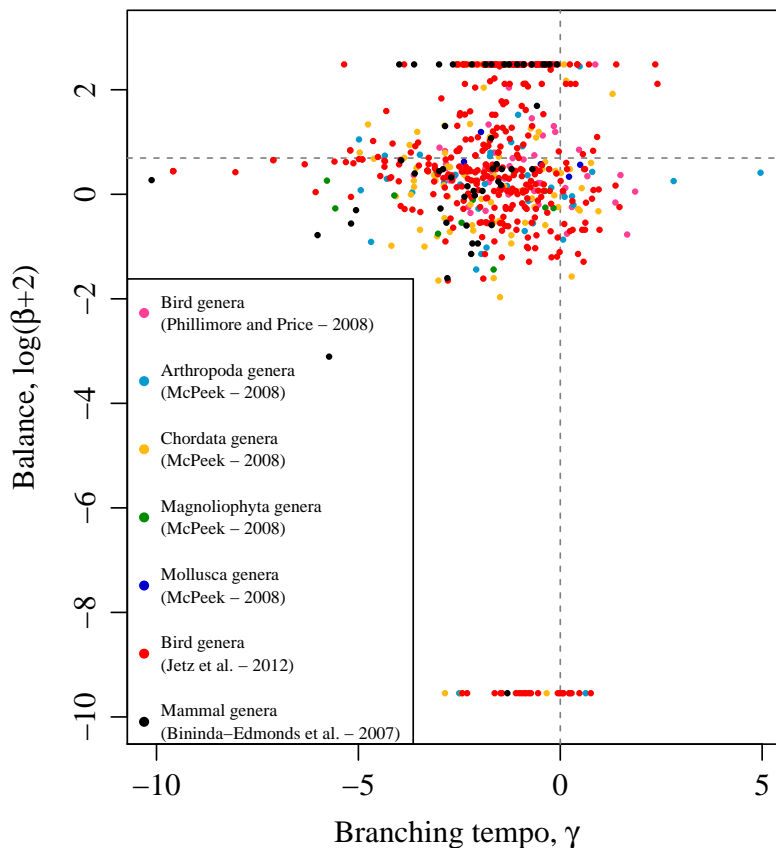
FIGURE A13 – Branching tempo γ and balance β for phylogenies of genera, compiled from published data. Vertical and horizontal dashed grey lines respectively show γ=0 and β=0. Colors are according to the taxonomic group and data set from which we extracted each phylogeny (Phillimore and Price 2008; McPeek 2008; Jetz et al. 2012; Bininda-Emonds et al. 2007).

*

References

Behm, J. E., A. R. Ives, and J. W. Boughman. 2010. Breakdown in postmating isolation and the collapse of a species pair through hybridization. Am. Nat. 175 :11–26.

Bininda-Emonds, O. R. P., M. Cardillo, K. E. Jones, R. D. E. MacPhee, R. M. D. Beck, R. Grenyer, S. A. Price, R. A. Vos, J. L. Gittleman, and A. Purvis. 2007. The delayed rise of present-day mammals. Nature 446 :507–512.

Blum, M. and O. François. 2006. Which random processes describe the tree of life? A large-scale study of phylogenetic tree imbalance. Syst. Biol. 55 :685–691.

Elowsky, C. G., I. E. Jordon-Thaden, and R. B. Kaul. 2013. A morphological analysis of a hybrid swarm of native Ulmus rubra and introduced U. pumila (Ulmaceae) in southeastern Nebraska. Phytoneuron 44 :1–23.

Gavrilets, S. 2003. Perspective : models of speciation : what have we learned in 40 years? Evolution 57 :2197–2215.

Guyer, C. and J. B. Slowinski. 1991. Comparison of observed phylogenetic topologies with null expectations among three monophyletic lineages. Evolution 45 :340–350.

Guyer, C. and J. B. Slowinski. 1993. Adaptive radiation and the topology of large phylogenies. Evolution 47 :253–263.

Harmon, L. J., J. T. Weir, C. D. Brock, R. E. Glor, and W. Challenger. 2008. GEIGER : investigating evolutionary radiations. Bioinformatics 24 :129–131.

Hasselman, D. J., E. E. Argo, M. C. McBride, P. Bentzen, T. F. Schultz, A. A. Perez-Umphrey, and E. P. Palkovacs. 2014. Human disturbance causes the formation of a hybrid swarm between two naturally sympatric fish species. Mol. Ecol. 23 :1137–1152.

Jetz, W., G. Thomas, J. Joy, K. Hartmann, and A. Mooers. 2012. The global diversity of birds in space and time. Nature 491 :444–448.

Kendall, D. 1948. On some modes of population growth leading to R. A. Fisher's logarithmic series distribution. Biometrika 35 :6–15.

Kleindorfer, S., J. A. O'Connor, R. Y. Dudaniec, S. A. Myers, J. Robertson, and F. J. Sulloway. 2014. Species collapse via hybridization in Darwin's tree finches. Am. Nat. 183 :325–341.

Matute, D. R., I. A. Butler, D. A. Turissini, and J. A. Coyne. 2010. A test of the snowball theory for the rate of evolution of hybrid incompatibilities. Science 329 :1518–1521.

McPeek, M. 2008. The ecological dynamics of clade diversification and community assembly. Am. Nat. 172 :E270–E284.

Mooers, A. O. 1995. Tree balance and tree completeness. Evolution 49 :379–384.

Moyle, L. C. and T. Nakazato. 2010. Hybrid incompatibility "snowballs" between Solanum species. Science 329 :1521–1523.

Nee, S., A. O. Mooers, and P. H. Harvey. 1992. Tempo and mode of evolution revealed from molecular phylogenies. Proc. Natl. Acad. Sci. USA 89 :8322–8326.

Orr, H. A. 1995. The population genetics of speciation : the evolution of hybrid incompatibilities. Genetics 139 :1805–1813.

Orr, H. A. and M. Turelli. 2001. The evolution of postzygotic isolation : accumulating Dobzhansky-Muller incompatibilities. Evolution 55 :1085–1094.

Phillimore, A. B. and T. D. Price. 2008. Density-dependent cladogenesis in birds. PLoS Biol. 6 :e71.

Pybus, O. G. and P. H. Harvey. 2000. Testing macro-evolutionary models using incomplete molecular phylogenies. Proc. R. Soc. Lond. B. 267 :2267–2272.

Rabosky, D. L. and D. R. Matute. 2013. Macroevolutionary speciation rates are decoupled from the evolution of intrinsic reproductive isolation in Drosophila and birds. Proc. Natl. Acad. Sci. USA 110 :15354–15359.

Raup, D. M., S. J. Gould, T. J. M. Schopf, and D. S. Simberloff. 1973. Stochastic models of phylogeny and the evolution of diversity. J. Geol. 81 :525–542.

Taylor, E. B., J. W. Boughman, M. Groenenboom, M. Sniatynski, D. Schluter, and J. L. Gow. 2006. Speciation in reverse : morphological and genetic evidence of the collapse of a three-spined stickleback (Gasterosteus aculeatus) species pair. Mol. Ecol. 15 :343–355.

Ungerer, M. C., S. J. Baird, J. Pan, and L. H. Rieseberg. 1998. Rapid hybrid speciation in wild sunflowers. Proc. Natl. Acad. Sci. USA 95 :11757–11762.

Yule, G. 1925. A mathematical theory of evolution, based on the conclusions of Dr. J. C. Willis, F.R.S. Philos. T. Roy. Soc. B. 213 :402–410.